small

Catalytic Nanomotors: Self-Propelled Sphere Dimers

*Leonardo F. Valadares, Yu-Guo Tao, Nicole S. Zacharia, Vladimir Kitaev, Fernando Galembeck, Raymond Kapral, and Geoffrey A. Ozin**

Experimental and theoretical studies of the self-propelled motional dynamics of a new genre of catalytic sphere dimer, which comprises a non-catalytic silica sphere connected to a catalytic platinum sphere, are reported for the first time. Using aqueous hydrogen peroxide as the fuel to effect catalytic propulsion of the sphere dimers, both quasi-linear and quasi-circular trajectories are observed in the solution phase and analyzed for different dimensions of the platinum component. In addition, well-defined rotational motion of these sphere dimers is observed at the solution–substrate interface. The nature of the interaction between the sphere dimer and the substrate in the aqueous hydrogen peroxide phase is discussed. In computer simulations of the sphere dimer in solution and the solution–substrate interface, sphere-dimer dynamics are simulated using molecular-dynamics methods and solvent dynamics are modeled by mesoscopic multiparticle collision methods taking hydrodynamic interactions into account. The rotational and translational dynamics of the sphere dimer are found to be in good accord with the predictions of computer simulations.

Keywords:
- mesoscopic dynamics
- nanomotors
- nanorotors
- particle–surface interactions
- sphere dimers

1. Introduction

Controlled motion of self-propelled nanoscale objects in solution and at interfaces represents a major goal in nanotechnology. Achieving this objective could provide the basis for lab-on-a-chip devices or drug delivery and cargo transport platforms.[1] A myriad of locomoting nanostructures that execute specific functions pervade the natural world. These miraculous nanomotors and nanomachines have been inspiring scientists to copy nature and create artificial tiny structures that can make specific movements.[2] Biomolecular-inorganic hybrids[3] and completely synthetic chemically powered nanostructures[4] have recently been reported but command over locomotion at the nanoscale remains a grand challenge for nanoscience and nanotechnology today. Most of the studies to date on chemically powered synthetic nanomotors have been carried out using catalytically propelled metallic nanorods. These devices are based on bimetallic nanorods,[5] such as Au–Pt or Au–Ni with one end inert and the other catalytic where the latter reacts with an energy-rich fuel such as H_2O_2. Usually linear nanorod motion is observed although both circular and rotational motion have been reported.[6]

Frequently, the movement of nanomotors is monitored over an underlying substrate like glass. Sometimes nanomotors are trapped and immobilized on the glass surface used for observation of the dynamics. One important factor often neglected is the interaction between the substrate and the nanomotors. Substrate–nanomotor electrostatic, hydrogen bonding, and hydrophobic interactions are expected to play an essential role in determining nanomotor mobility.[7]

Various explanations have been proposed for the origin of the motion of synthetic self-propelled objects. The mechanisms responsible for self-propulsion will depend on the nature, size,

---

[*] Prof. G. A. Ozin, Dr. Y.-G. Tao, Prof. R. Kapral
Department of Chemistry, University of Toronto
80 St. George Street, Toronto, Ontario, M5S 3H6 (Canada)
E-mail: gozin@chem.utoronto.ca

Dr. L. F. Valadares, Prof. F. Galembeck
Institute of Chemistry, Universidade Estadual de Campinas
P.O. Box 6154, Campinas, São Paulo, 13083-970 (Brazil)

Prof. N. S. Zacharia
Department of Mechanical Engineering, Texas A&M University
3123 TAMU, College Station, TX 77840 (USA)

Prof. V. Kitaev
Chemistry Department, Wilfrid Laurier University
75 University Ave. W., Waterloo, Ontario, N2L 3C5 (Canada)

Supporting Information is available on the WWW under http://www.small-journal.com or from the author.

DOI: 10.1002/smll.200901976

Final page numbers not assigned

and architecture of the constituents of a synthetic nanomotor. Proposed mechanisms include bubble detachment,[8] interfacial tension gradients,[4] gravitational forces,[9] diffusiophoretic driving,[10] and electrokinetic pumping.[11] These proposed driving forces can work together to impel the motors.[12]

Recently, theoretical investigations have been carried out on the motion of simple model sphere-dimer nanomotors[13] consisting of attached catalytic and non-catalytic spheres under non-equilibrium steady-state conditions. The self-propulsion of the model nanosphere dimer relies on the existence of a non-equilibrium density of product molecules produced in the reaction at the catalytic sphere and a difference in the interaction forces between the two types of sphere and the product molecules. Molecules produced by reaction on the surface of the catalytic sphere diffuse in solution and give rise to a concentration gradient over the surface of the non-catalytic sphere. The net force on the non-catalytic sphere is non-zero due to the variation of the concentration over the sphere surface, which this leads to propulsion. This mechanism depends directly on the intermolecular forces between the motor and the chemical species participating in the reaction at the catalytic sphere. It is these forces that underlie macroscopic properties such as the surface tension. The macroscopic counterpart of our mechanism is the diffusiophoretic driving of the motor.[10] The analysis and simulation of this simple motor allow one to assess the relative importance of key factors, many of which are independent of the details of the propulsion mechanism, which determine the velocity. These factors include sphere sizes, chemical reaction rates, dimer internuclear separation, and solvent viscosity. The self-propelled motion of sphere-dimer motors can be controlled easily by varying the sizes of the two spheres, as well as their internuclear separation, in order to modify the magnitude of the chemical gradient that is an essential element in the propulsion mechanism. The fact that the chemical gradient can be controlled by fabrication makes these motors ideal candidates for the exploration of chemically powered motor design in order to enhance self-propelled motion.

This theoretical modeling has encouraged us to design and experimentally study a silica–platinum sphere-dimer nanomotor whose directional motion dominates over the Brownian thermal fluctuations. Herein we present for the first time an experimental study of these autonomously moving sphere dimers and analyze the results with the aid of simulations on model sphere dimers.

2. Results and Discussion

2.1. Synthesis and Structure of the Sphere Dimers

The Experimental Section gives the complete procedure used to fabricate the sphere dimers. The method is based on deposition of a sub-monolayer of silica microspheres on flat silicon/platinum substrates, followed by a thin adhesion layer of chromium and finally a thicker platinum layer. On annealing the samples, the metallic half-shells de-wet, forming an attached platinum particle over each silica sphere.[14] Figure 1 shows a scheme of this method. Platinum layers of many thicknesses (25, 40, 55, 70, or 85 nm) were used to obtain the samples named *a*, *b*, *c*, *d*, or *e*, respectively.

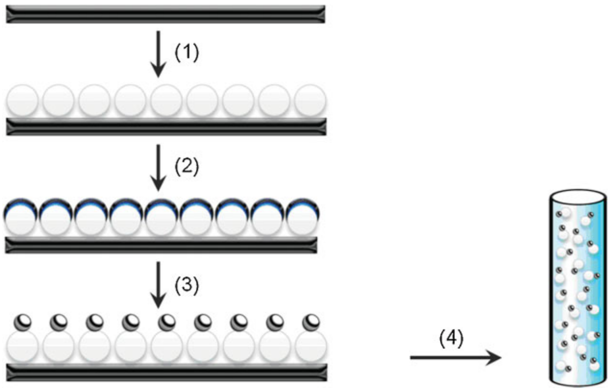

Figure 1. Scheme showing the synthesis of the sphere dimers. 1) Silica sub-monolayer deposition over the substrate. 2) Metallic half-shell deposition over the silica beads: a 5-nm chromium adhesion layer was first sputtered followed by a platinum thicker layer. 3) Thermal annealing at 900 °C for 3 h. 4) Redispersion of sphere dimers in water by sonication.

The sphere dimers were first characterized prior to the dynamics measurements. Figure 2 shows scanning electron microscopy (SEM) images of sample *a* (Figure 2a), sample *c* (Figure 2b), and sample *e* (Figure 2c), in which the substrates were tilted to provide a perspective view of the silica–platinum sphere dimers. After the thermal annealing, the silica microspheres maintain their spherical shape, however, the metallic hemi-layers become approximately spherical due to the high platinum surface tension and high platinum–silica interface tension. Table 1 shows the results of the sphere-dimer structural characterization. The diameters of the platinum particles were measured in a batch of at least 350 particles for each sample from top-view SEM images (Figure 3a–e). Figure 3f shows the distribution of the platinum particle diameters for these samples. The distribution of sizes of the platinum particles is not monodisperse, even though the diameters of these particles depend on the thickness of the metallic hemi-layer sputtered onto the silica microspheres. This approach creates a large yield of silica–platinum sphere dimers

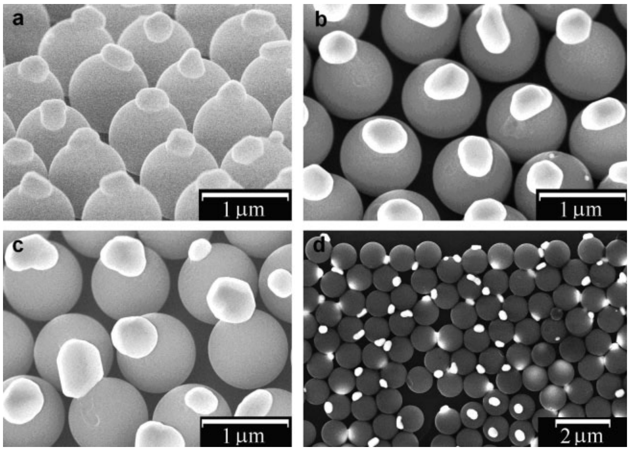

Figure 2. SEM images of sphere dimers. a) Sample *a* (tilt angle 60°). b) Sample *c* (tilt angle 30°). c) Sample *e* (tilt angle 30°). d) Sphere dimers from sample *a* after they had been released from the substrate and redeposited on a carbon-coated surface.

Table 1. Structure and speed of the sphere dimers. Structural characteristics and mean speed of sphere dimers when immersed in 15% H_2O_2 solution. The errors represent the standard deviation of the measurement.

Sample	Pt layer thickness [nm]	Pt particle diameter [nm]	Percentage of sphere dimers in the sample [%]	Average speed of the sphere dimers in 15% H_2O_2 solution [$\mu m\ s^{-1}$]
a	25	325 ± 30	75.1	2.5 ± 0.2
b	40	368 ± 30	85.3	3.5 ± 1.4
c	55	417 ± 35	71.2	5.1 ± 1.7
d	70	448 ± 41	80.9	6.0 ± 4.0
e	85	489 ± 50	42.2	5.6 ± 3.7

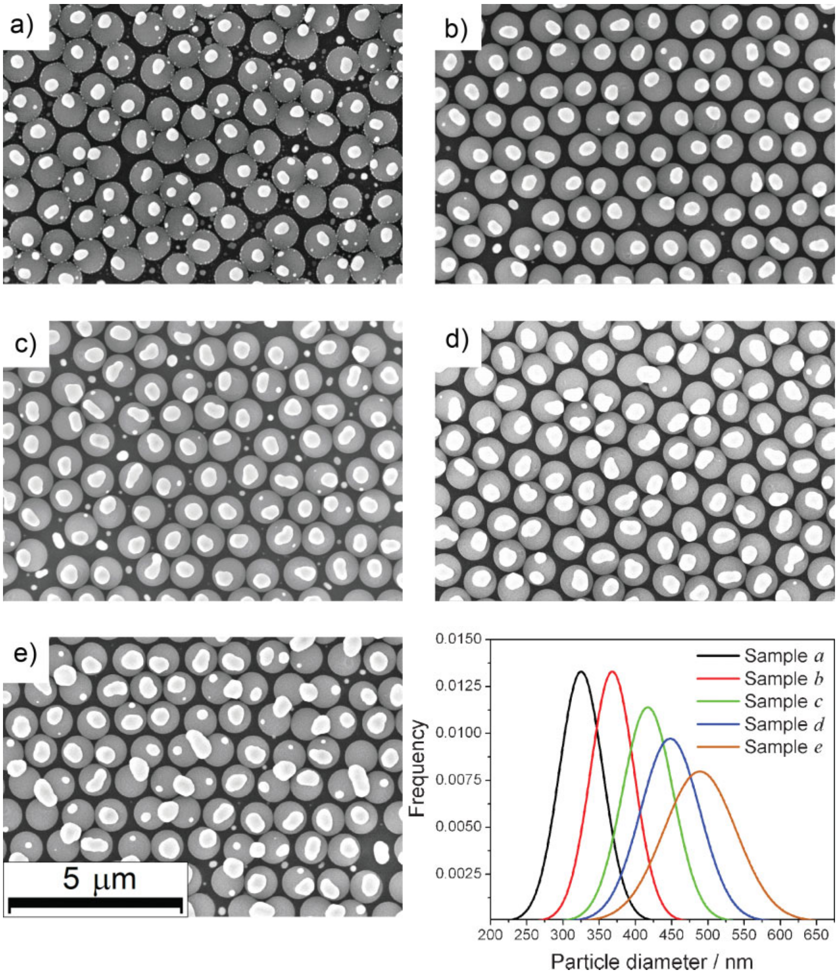

Figure 3. SEM top-view images of sphere dimers over silicon substrates. The samples were prepared with platinum layers of different thicknesses: a) sample *a*, 25 nm, b) sample *b*, 40 nm, c) sample *c*, 55 nm, d) sample *d*, 70 nm, and e) sample *e*, 85 nm. f) Distributions of the diameter of the platinum particle in these samples.

(Table 1), but occasionally two platinum particles are formed over the same silica microsphere, and sometimes a large platinum particle de-wets between two silica microspheres, a behavior that predominates when using thicker platinum hemi-layers (≥85 nm). These adventitious particles are not included in our dynamics measurements to be described below.

We could easily redisperse the silica–platinum sphere dimers when synthesized over platinum substrates simply by immersing them in water and sonicating them briefly. Figure 2d shows sphere dimers from sample *a* that had been released from the platinum substrate. The silica–platinum sphere-dimer structure is maintained after release without breaking the necks of the particles as a consequence of platinum and silica adhesion mediated by chromium.

2.2. Motion of the Sphere Dimers

The sphere dimers were diluted in water and mixed with H_2O_2 solution to obtain dispersions with defined concentrations. These dispersions were immediately placed in chambered cover slides and were analyzed in an inverted microscope using the transmission light observation mode. The objective lens focus was arranged to be on top of the glass surface and thereby analyzed the 2D motion. By taking a sequence of images at regular time intervals, the movement and orientation of sphere dimers were tracked by the position of the platinum and silica particles in each frame.

The platinum particle catalyzes the surface chemical reaction: $2H_2O_2 \rightarrow O_2 + 2H_2O$. This reaction is responsible for propulsion of the sphere dimers. Table 1 shows the average speed of the sphere dimers determined from the silica sphere displacement. The average speed of sphere dimers in 15% H_2O_2 solution is significantly increased when compared to the speed measured under the same conditions for the sample *c* in water, which is $2.0 \pm 0.2\ \mu m\ s^{-1}$. For the same silica sphere size, the sphere-dimer speed increases with the platinum particle size, and then plateaus or even decreases slightly as the platinum–silica sphere diameter ratio increases further. The highest average speed is observed for sample *d* with a platinum particle diameter of 448 nm, although the error estimates are large and a plateau in the speed with increasing platinum particle diameter cannot be ruled out.

Sphere dimers from the same sample move with different velocities, resulting in a high standard deviation measured for the speed. This is not unexpected considering that the sphere

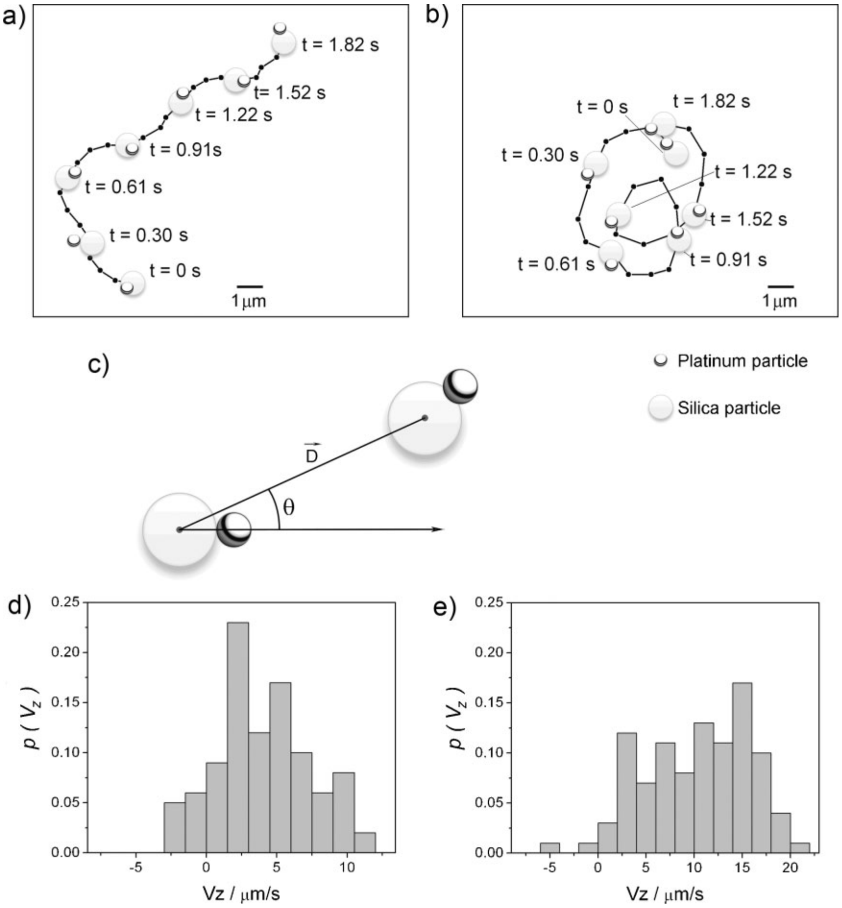

Figure 4. Motion of free sphere dimers in aqueous H_2O_2 solution: a) quasi-linear trajectory and b) quasi-circular trajectory. Plots (black circles and lines) show the trajectory of the silica sphere. The spheres represent the silica (bigger) and the platinum (smaller) particles to show the orientation of sphere dimers from sample *c* in aqueous 15% H_2O_2 solution. c) Scheme illustrating the calculation of velocity of the silica sphere along the sphere-dimer internuclear axis, $V_z = \left|\vec{D}\right| \cos\theta/\Delta t$. Here $\vec{D}$ gives the displacement of the silica sphere over one time interval Δt and θ is the initial angle between the intersphere axis and the displacement vector. d) Probability distribution of V_z of the sphere dimer shown in (a). e) Probability distribution of V_z of the sphere dimer shown in (b).

dimers from the same batch do not have perfectly uniform platinum particles sizes (Figure 3) upon which the speed is dependent. Another factor that can influence the speed is the interaction of sphere dimers with the surface of the underlying glass substrate. Figure 4 shows sample trajectories of sphere dimers in H_2O_2 solution: namely quasi-linear (Figure 4a) and quasi-circular (Figure 4b) modes are observed. Supplementary Video 1 and Supplementary Video 2 show the real time motion of these sphere dimers, respectively. The sphere dimers are propelled in the direction of the attached catalytic platinum particle. The direction of the observed motion is opposite to that predicted by the bubble detachment mechanism.[8] The motion of sphere dimers can be monitored best by computing the velocity of the silica sphere along the sphere-dimer internuclear axis, V_z (Figure 4c). Positive values of V_z represent the displacement of sphere dimer in the direction of the catalytic platinum particle and the average V_z is zero for Brownian motion. The propelled sphere dimers clearly describe directed motion as is evident from the non-zero values of V_z. Figure 4d and e shows the recorded histograms of the velocity of the sphere dimers presented in Figure 4a and b, respectively. The velocity V_z shows the same variation with platinum particle size as the silica particle speed reported in Table 1.

The above results show that the self-propelled motion exhibits two main features: there is directed motion along the internuclear axis but it is strongly affected by Brownian motion as expected for nanoscale motors, and the mean motor velocity increases and then plateaus or even decreases with increasing platinum–silica sphere diameter ratio, d_C/d_N, where d_C and d_N represent the diameter of the catalytic and non-catalytic particles, respectively. Both of these effects are captured by simulations on the model dimer.

The simulated V_z probability distribution function, $p(V_z)$, of a model sphere dimer with a diameter ratio of $d_C/d_N = 0.5$ is shown in Figure 5a. As in the experimental Figure 4d and e, the probability distribution shows self-propelled motion in the direction of the catalytic sphere with significant broadening due to Brownian motion. As shown in Supplementary Video 3, the sphere dimer is found to translate many times its body length before reorientation. The rotational-diffusion component depends on the dimer size: a sphere dimer with small size will reorient rapidly since the rotational-diffusion coefficient scales as the inverse of the cube of the characteristic size. The quasi-circular trajectories seen in some of the experiments likely arise from both rotational Brownian motion and, more importantly, from asymmetries in the catalytic platinum particles, as discussed below.

The dependence of the mean velocity on the sphere diameter ratio is also explained by the model simulations and analysis. Figure 5b plots the simulated average velocities of the sphere dimers as a function of the diameter ratio. The dependence of V_z on the diameter ratio shows a variation similar to that in the experimental data in Table 1. An analysis of the model equations[13b] that determine the dimer velocity shows that it depends on a number of important competing factors. For a fixed diameter of the non-catalytic sphere, initially, as the catalytic sphere diameter increases, the reaction rate increases due to the increased surface area of the catalytic sphere. Since the reaction rate depends on the catalytic surface area, the enhanced production of product molecules leads to an increase in the propulsion velocity.[15] However, this increase cannot persist since further increases in the catalytic sphere diameter will lead to an increase of the frictional force on the dimer, which will decrease its velocity. The hydrodynamic component of the friction will increase roughly linearly with the

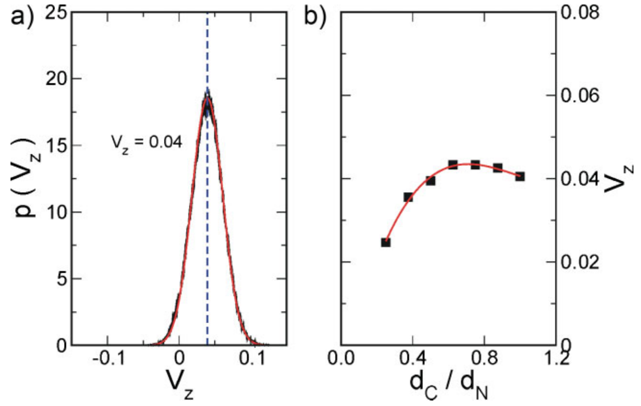

Figure 5. The average velocity of the model sphere dimer in simulation units. a) Probability distribution function. The non-catalytic sphere diameter is twice that of the catalytic sphere. b) Sphere-dimer velocity as a function of the ratio of the size of the catalytic and non-catalytic constituent sphere diameters, d_C/d_N. Simulation results are obtained by fitting the probability distribution function, $p(V_z)$, averaged over 10 independent realizations to a Maxwell–Boltzmann distribution, as shown in panel (a).

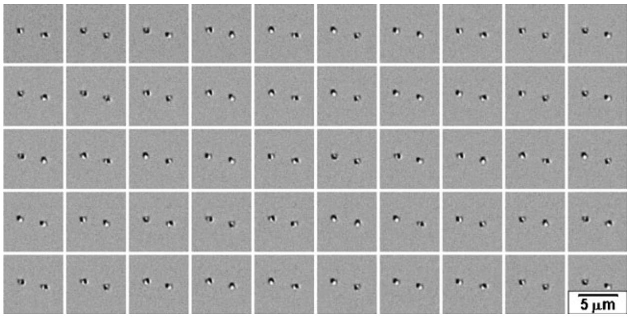

Figure 6. Sphere dimers rotating over the glass surface. Consecutive time frames obtained in an inverted optical microscope showing sphere dimers of sample *e* in 15% H_2O_2 undergoing rotation: the silica sphere (white spot) is attached to the glass surface and the platinum sphere (dark spot) is rotating. The sphere dimer on the left describes counterclockwise rotation at 1.5 Hz and the sphere dimer on the right describes clockwise rotation at 3.6 Hz. The time between frames is 76 ms.

diameter of the sphere. In addition, as the catalytic sphere diameter increases and becomes large or comparable in size to that of the non-catalytic sphere, the non-equilibrium gradient of product molecules across the non-catalytic sphere will be reduced[13b] and this, in turn, will also tend to reduce the dimer velocity. Finally, in addition to the trends described above that depend on the relative values of the velocity for different platinum particle sizes, we note that using the scaling between simulation units and physical units discussed earlier, the model dimer velocities range from $V_z = 3.9$ to $6.9\ \mu\text{m s}^{-1}$, which are comparable to those seen in the experiments. Given that the model does not describe the detailed chemistry in the experiments and the fact that the platinum particles in the experiment are not perfectly spherical and the ensemble of sphere dimers not perfectly monodisperse, this agreement is very satisfactory.

During the measurements of the sphere-dimer dynamics, a distinctive behavior was observed, namely, the silica sphere is able to interact with the surface of the glass substrate while the platinum particle then rotates freely, resembling the motion of a satellite. These sphere-dimer rotors were observed in all samples used in this study. The sphere dimers rotate both clockwise and counterclockwise, as shown in Figure 6 and in Supplementary Video 4. The direction of rotation is random. The revolution speed of sphere dimers was clocked and found to remain constant for several minutes for the same rotor. However, the rotation frequency varies among sphere-dimer batches and among different sphere dimers from the same batch. Interestingly, sphere-dimer rotors are only observed over pristine untreated glass surfaces and these rotors always interact with the glass surface through the silica particle.

The rotational movement clearly originates when a sphere dimer becomes anchored to the glass surface. The main forces acting between the sphere dimers and the surface are believed to arise from electrostatic, hydrogen-bonding, and van der Waals interactions. Under reaction conditions the glass substrate and the silica sphere surfaces are both negatively charged and the electrostatic forces acting between them are long-range repulsive. These forces prevent close contact between the surfaces. By contrast, the van der Waals forces are attractive at shorter ranges. This type of force is very strong for surfaces with similar composition,[16] which is the case for the surface of the silica sphere and glass substrate (borosilicate). These surfaces are also expected to interact via hydrogen bonds between silanol groups located on both surfaces, thereby trapping the silica sphere at a particular location on the glass substrate. The hydrogen bonding can be mediated by water molecules. We believe that a strong local attraction takes place between a small patch of the silica sphere and the glass surface, impeding the displacement of the silica sphere but allowing the rotation of the sphere dimer, as observed in practice. By contrast, the platinum particle is expected to be weakly attracted to the glass surface as van der Waals forces are weaker for dissimilar compositions and surface hydroxyl groups needed for hydrogen bonding are likely to be less prominent via the platinum particle surface.

During the observation of the nanorotor motion it was not possible to investigate the particular morphology of a sphere dimer due to the limited resolution of optical microscopy, however, the results suggest that the rotational movement is due to the asymmetry of the sphere dimers with respect to its silica–platinum interparticle axis. This asymmetry arises from the irregular shape of the attached platinum particles and might be also affected by the different catalytic activities of platinum crystalline planes. Another possibility is the breaking of symmetry as a result of a gradient of concentration along the platinum catalyst particle created by the motion itself.

Simulations of the model sphere-dimer motor allow one to investigate factors leading to directed rotational motion of dimers attached to a surface. Since the rotational motion of the surface-attached sphere dimer is likely caused by the asymmetry of the catalytic particle, we have modeled the rotational dynamics as follows: the center of mass of the non-catalytic sphere was immobilized at a fixed distance from one point on the surface of the wall so that translational motion was suppressed. The sphere dimer is still free to execute rotational motion. If the entire catalytic sphere surface is uniformly catalytic as in the translational simulations described above, no persistent unidirectional rotational motion is observed. Only rotational Brownian motion is seen. In the experiment, the platinum catalytic particles are irregular, as seen in Figures 2 and 3. Consequently, one expects that the catalytic activity will not be uniform over the entire surface of the catalytic particles. To model such asymmetry, we made the catalytic sphere in the dimer a small Janus sphere that has hemispherical catalytic and non-catalytic halves. Chemical reaction occurs at the catalytic side of the Janus sphere, which produces an asymmetric non-equilibrium gradient of the product molecule density in the vicinity of the small sphere (Figure 7a). Figure 7b shows the corresponding symmetric case for comparison. A persistent unidirectional rotational motion of the sphere dimer is now observed, as can been seen in Supplementary Video 5, in accord with experimental observations. The direction of rotation, clockwise or counterclockwise, depends on the location of the active catalytic portion of the Janus sphere.

We note with interest the existence of some aggregates of sphere dimers in the dispersion forming tetramers, hexamers, or even more complexes structures. In these sphere-dimer aggregates the contact point is through the silica spheres. Supplementary Video 6 shows a sphere tetramer moving over the glass surface in 10% H_2O_2 solution. The tetramer motion moving at 5.0 μm s^{-1} is relatively linear in the direction of the platinum particles. Supplementary Video 7 presents the motion of a hexamer in 10% H_2O_2 solution. In this case, the hexamer describes a circular motion and its constituent sphere dimers are perpendicularly aligned with respect to the glass surface. These preliminary results on self-propelled motional dynamics of aggregated sphere-dimer structures show that their movement and orientation depend on shape. This topic is reserved for future investigations.

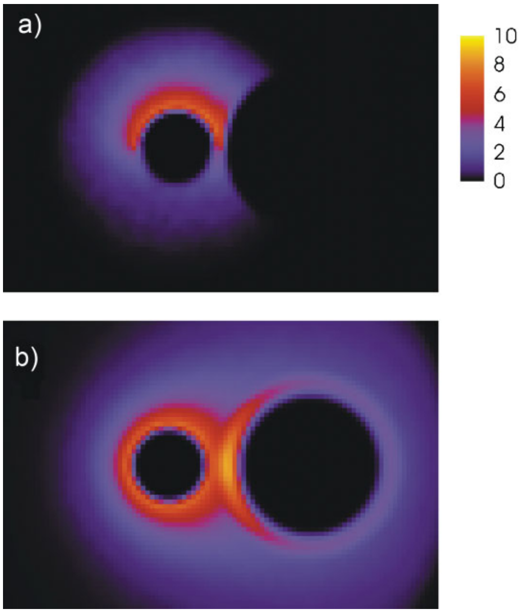

Figure 7. The average number density profile of *B* product molecules in the vicinity of a) the sphere-dimer nanorotor and b) the sphere-dimer linear nanomotor. The *B* molecules are taken from a 24 × 16 × 1 slice parallel to the dimer internuclear axis and the solid walls. The total density field is approximately uniform, while the gradient of the *B* molecule field in the vicinity of the dimer (rotor) is evident.

3. Conclusions

In this paper, experimental and theoretical investigations of the self-propelled and Brownian motional dynamics of model catalytic sphere dimers composed of silica and platinum building blocks have been reported for the first time. Both quasi-linear and quasi-circular trajectories have been observed in H_2O_2 solution and analyzed for different dimensions of sphere dimers. In addition, well-defined rotational motion of sphere dimers tethered to the underlying glass substrate has been observed. The nature of the interaction between sphere dimer and substrate has been discussed and the rotational dynamics of the sphere dimer have been analyzed.

The sphere dimers described in this study are expected to find applications as building blocks to fabricate new types of dynamic structures and devices.[17] In future work, it is possible that ways can be found to judiciously interconnect sphere dimers and probe the effect of shape on the dynamics. In this context, it will be important to utilize synthetic methods for the large-scale production of sphere dimers, as recently described.[18] An extension of this concept is to make sphere trimers and tetramers with different sizes and shapes and location of the catalytic sphere. Furthermore, the use of surface-patterning techniques such as soft lithography can be used to assemble various arrangements of tethered sphere-dimer motors to achieve directional motion or to synchronize the actions of an ensemble of particles. Ultimately, one would like to put catalytic nanomotors to work by giving them practical tasks exemplified by picking up and delivering chemical payloads in microfluidic chips, eliminating pollution in rivers and streams, and even removing toxic chemicals within our bodies and performing medical procedures on organs and cells.

4. Experimental Section

Materials and methods: Sphere dimers were prepared using the method described by Lu et al.[14] adapted to work with platinum. The method consists of dispersing silica spheres over an inert substrate followed by deposition of a chromium adhesion layer over the silica and a thicker layer of platinum over the chromium. Annealing the system causes the metallic half-shell[19] to de-wet from the silica, thereby forming a metal particle attached to one side of the silica sphere. Figure 1 shows a scheme of this synthetic method.

Silicon and platinum-covered silicon were used as substrates. Silicon substrates were cleaned with Piranha solution (3:1 H_2SO_4 conc./H_2O_2 30%) (*CAUTION: Piranha solution can react violently with organic compounds*) followed by rising in water and ethanol. To cover the substrates with platinum, a 5-nm chromium layer was first sputtered over clean silicon substrates followed by a 200-nm platinum layer. Samples prepared over silicon wafers were used for field-emission SEM (Hitachi S-5200) analyses. The sphere dimers prepared over platinum-covered substrates were redispersed in water and used for the dynamics analyses because they were most easily released into solution.

Sub-monolayers of 970-nm silica spheres were prepared by dip-coating the substrates in a 0.05 v/v silica/ethanol dispersion using 100 mm min^{-1} immersion and removal rates. A 5-nm chromium adhesion layer was first sputtered onto these sub-monolayers of silica spheres, followed by a thicker platinum layer. Different samples were prepared using the following platinum layer thicknesses: 25, 40, 55, 70, or 85 nm. These samples were named *a*, *b*, *c*, *d*, and *e*, respectively. A Perkin-Elmer 2400 sputtering system was used for metal deposition. The sputter-coated silica spheres were annealed at 900 °C for 3 h under air atmosphere using a 10 °C min^{-1} heating rate. The sphere dimers prepared on platinum-coated silicon substrates were redispersed by immersing samples in water and sonicating for 10 s.

The sphere-dimer dispersions were diluted to $\approx 10^8$ dimers L^{-1} and usually a 1:1 mixture of sphere-dimer dispersion and aqueous H_2O_2 was used for dynamics studies. In this mixture, both original constituents were diluted by half. Then 0.2 mL of this mixture was placed in the chambered cover glass (Nunc Lab-Tec). The chambered cover slides were previously sonicated in water and ethanol to clean the glass surface.

The motion of the sphere dimers was observed and recorded using a 63× objective oil lens on a Zeiss inverted microscope (Axiovert) fitted with a Photometric Cool Snap camera. The lens was focused at the glass surface and 2D sphere-dimer motion was analyzed. In vivo software was used for imaging. Image-Pro Plus software was used for image edition and sphere-dimer tracking. Usually 100 frames were acquired over 7.6 s, namely, $\approx$13 frames s^{-1}. Ten moving sphere dimers were tracked to obtain the average speed of each sample. The finite-time approximation to the speed was calculated from the ratio of the silica sphere displacement to the time between each frame.

Simulations: In the simulations, the sphere dimer was immersed in a solution containing point-like *A* and *B* molecules. The system was confined to a cubic box with two solid walls in the *z*-direction, while periodic boundary conditions were used in the *x*- and *y*-directions. The dimer spheres interact with the walls though 9–3 Lennard–Jones (LJ) potentials

$$V_{\text{LJ}}^{93}(r) = \varepsilon_{\text{w}}[(\sigma_{\text{w}}/r)^9 - (\sigma_{\text{w}}/r)^3] \tag{1}$$

where ε_{W} and σ_{W} are wall energy and distance parameters, respectively, and *r* is the distance of the particle from the wall or the internuclear distance between particles. These distance and energy parameters were adjusted so that the sphere dimer resides at locations close to the lower wall. This mimics the experiments where the dimer motion is near the surface of the glass cover slide. The *A* molecules interact with both spheres through a truncated repulsive LJ potential

$$V_{\text{LJ}}^{\text{R}}(r) = 4\varepsilon_{\text{A}}[(\sigma_{\text{S}}/r)^{12} - (\sigma_{\text{S}}/r)^6 + 1/4] \tag{2}$$

at $r < r_{\text{c}}$, where $r_{\text{c}} = 2^{1/6}\sigma_{\text{S}}$ is the cut-off distance. The *B* molecules interact with the catalytic (C) sphere through the same repulsive LJ potential, but interact with the non-catalytic (N) sphere through an attractive LJ potential

$$V_{\text{LJ}}^{\text{A}}(r) = 4\varepsilon_{\text{B}}[(\sigma_{\text{N}}/r)^{12} - (\sigma_{\text{N}}/r)^6]s(r) \tag{3}$$

where *s*(*r*) is a switching function that smoothly truncates the potential to zero. The dynamics of the sphere dimers are simulated by standard molecular dynamics, while the solvent dynamics are modeled by mesoscopic multiparticle collision dynamics,[20] which properly account for hydrodynamic interactions. Solvent molecules interact with the walls by bounce-back boundary conditions where their velocities are reversed on collision. The chemical reaction, $A + C \rightarrow B + C$, occurs when *A* solvent molecules come close enough to the catalytic sphere. In order to maintain a non-equilibrium steady state, *B* molecules are converted back to *A* species when they diffuse far enough away from the catalytic sphere. This mimics the fluxes of solvent molecules into and out of the system that maintain it out of equilibrium. As in the experiments, the diameter of the non-catalytic sphere was fixed and the catalytic sphere diameter was varied. Although the simple dimer model is not intended to describe the detailed kinetics of the silica–platinum sphere-dimer motor, it captures many generic features of chemically powered self-propelled motion and is used to identify and explain important qualitative trends seen in the experimental data. Computational results are reported in dimensionless simulation units. However, by matching the non-catalytic sphere size in the simulation to that of the silica sphere ($\approx$1 μm) in the experiment and using the viscosity of water at room temperature ($\approx$1 mPa · s) in conjunction with the theoretical value of the viscosity[20] in the mesoscopic simulations to extract the time scale, dimensionless simulation units can be mapped onto physical units.

Acknowledgements

G.A.O. is a Government of Canada Research Chair in Materials Chemistry and Nanochemistry. He is deeply indebted to the Natural Sciences and Engineering Research Council (NSERC) of Canada for strong and sustained financial support of his work. Research by Y.-G.T. and R.K. is supported in part by a grant from the NSERC of Canada. V.K. acknowledges WLU and NSERC support. F.G. acknowledges INCT Inomat. L.F.V. was supported by a CAPES fellowship from the Brazilian Government. The inverted optical microscopy measurements were performed in the Advanced Optical Microscopy Facility (AOMF). The authors are grateful to Ludovico Cademartiri for valuable discussions.

---

[1] a) G. A. Ozin, I. Manners, S. Fournier-Bidoz, A. C. Arsenault, *Adv. Mater.* **2005**, *17*, 3011–3018; b) T. E. Mallouk, A. Sen, *Sci. Am.* **2009**, *300*, 72–77; c) J. Wang, *ACS Nano* **2009**, *3*, 4–9.

[2] K. Oiwa, H. Kojima, *Nat. Nanotechnol.* **2008**, *3*, 531–532.

[3] R. K. Soong, G. D. Bachand, H. P. Neves, A. G. Olkhovets, H. G. Craighead, C. D. Montemagno, *Science* **2000**, *290*, 1555–1558.

[4] W. F. Paxton, K. C. Kistler, C. C. Olmeda, A. Sen, S. K. St, Angelo, Y. Cao, T. E. Mallouk, P. E. Lammert, V. H. Crespi, *J. Am. Chem. Soc.* **2004**, *126*, 13424–13431.

[5] S. R. Nicewarner-Peña, R. G. Freeman, B. D. Reiss, L. He, D. J. Peña, I. D. Walton, R. Cromer, C. D. Keating, M. J. Natan, *Science* **2001**, *294*, 137–141.

[6] a) S. Fournier-Bidoz, A. C. Arsenault, I. Manners, G. A. Ozin, *Chem. Commun.* **2005**, *441* . 443; b) L. Qin, M. J. Banholzer, X. Xu, L. Huang, C. A. Mirkin, *J. Am. Chem. Soc.* **2007**, *129*, 14870–14871; c) Y. Wang, S.-t. Fei, Y.-M. Byun, P. E. Lammert, V. H. Crespi, A. Sen, T. E. Mallouk, *J. Am. Chem. Soc.* **2009**, *131*, 9926–9927.

[7] S. K. St. Angelo, C. C. Waraksa, T. E. Mallouk, *Adv. Mater.* **2003**, *15*, 400–402.

[8] a) Y. Mei, G. Huang, A. A. Solovev, E. B. Ureña, I. Mönch, F. Ding, T. Reindl, R. K. Y. Fu, P. K. Chu, O. G. Schmidt, *Adv. Mater.* **2008**, *20*, 4085–4090; b) A. A. Solovev, Y. Mei, E. B. Ureña, G. Huang, O. G. Schmidt, *Small* **2009**, *5*, 1688–1692; c) J. G. Gibbs, Y.-P. Zhao, *Appl. Phys. Lett.* **2009**, *94*, 163104.

[9] N. I. Kovtyukhova, *J. Phys. Chem. C* **2008**, *112*, 6049–6056.

[10] R. Golestanian, T. B. Liverpool, A. Ajdari, *Phys. Rev. Lett.* **2005**, *94*, 220801(4).

[11] a) Y. Wang, R. M. Hernandez, D. J. Bartlett, J. M. Bingham, T. R. Kline, A. Sen, T. E. Mallouk, *Langmuir* **2006**, *22*, 10451–10456; b) R. Laocharoensuk, J. Burdick, J. Wang, *ACS Nano* **2008**, *5*, 1069–1075; c) U. K. Demirok, R. Laocharoensuk, K. M. Manesh, J. Wang, *Angew. Chem. Int. Ed.* **2008**, *47*, 9349–9351.

[12] T. Mirkovic, N. S. Zacharia, G. D. Scholes, G. A. Ozin, *Small* **2010**, *6*, 159.

[13] a) G. Rückner, R. Kapral, *Phys. Rev. Lett.* **2007**, *98*, 150603; b) Y.-G. Tao, R. Kapral, *J. Chem. Phys.* **2008**, *128*, 164518.

[14] Y. Lu, H. Xiong, X. Jiang, Y. Xia, M. Prentiss, G. M. Whitesides, *J. Am. Chem. Soc.* **2003**, *125*, 12724–12725.

[15] N. S. Zacharia, Z. S. Sadeq, G. A. Ozin, *Chem. Commun.* **2009**, *39*, 5856–5858.

[16] J. N. Israelachvili, in *Intermolecular and Surface Forces*, 3rd ed., Academic Press, San Diego, CA **1989**, Ch. 11.

[17] R. F. Ismagilov, A. Schwartz, N. Bowden, G. M. Whitesides, *Angew. Chem. Int. Ed.* **2002**, *41*, 652–654.

[18] A. Ohnuma, E. C. Cho, P. H. C. Camargo, L. Au, B. Ohtani, Y. Xia, *J. Am. Chem. Soc.* **2009**, *131*, 1352–1353.

[19] J. C. Love, B. D. Gates, D. B. Wolfe, K. E. Paul, G. M. Whitesides, *Nano Lett.* **2002**, *87*, 891–894.

[20] R. Kapral, *Adv. Chem. Phys.* **2008**, *140*, 89–146.

Received: October 20, 2009